AGU PUBLICATIONS

JGR

Journal of Geophysical Research: Space Physics

RESEARCH ARTICLE
10.1002/2017JA024551

Special Section:
Magnetospheric Multiscale (MMS) Mission Results Throughout the First Primary Mission Phase

Key Points:
- Intense lion roars are observed in mirror modes by high time resolution instruments on board Magnetospheric MultiScale mission
- Nonlinear lion roars are observed up to $0.4f_{ce}$ due to their high amplitude, which may have been underestimated in previous studies
- Possible signatures of linear and nonlinear resonant interaction between lion roars and electrons, which can be untrapped from mirror modes

Correspondence to:
H. Breuillard,
hbreuill@gmail.com

Citation:
Breuillard, H., Le Contel, O., Chust, T., Berthomier, M., Retino, A., Turner, D. L., … Fennell, J. F. (2018). The properties of lion roars and electron dynamics in mirror mode waves observed by the Magnetospheric MultiScale mission. *Journal of Geophysical Research: Space Physics*, *123*, 93–103. https://doi.org/10.1002/2017JA024551

Received 1 JUL 2017
Accepted 21 NOV 2017
Accepted article online 27 NOV 2017
Published online 3 JAN 2018

The Properties of Lion Roars and Electron Dynamics in Mirror Mode Waves Observed by the Magnetospheric MultiScale Mission

H. Breuillard[1], O. Le Contel[1], T. Chust[1], M. Berthomier[1], A. Retino[1], D. L. Turner[2], R. Nakamura[3], W. Baumjohann[3], G. Cozzani[1], F. Catapano[1], A. Alexandrova[1], L. Mirioni[1], D. B. Graham[4], M. R. Argall[5], D. Fischer[3], F. D. Wilder[6], D. J. Gershman[7], A. Varsani[3], P.-A. Lindqvist[8], Yu. V. Khotyaintsev[4], G. Marklund[8], R. E. Ergun[6], K. A. Goodrich[6], N. Ahmadi[6], J. L. Burch[9], R. B. Torbert[5], G. Needell[5], M. Chutter[5], D. Rau[5], I. Dors[5], C. T. Russell[10], W. Magnes[3], R. J. Strangeway[10], K. R. Bromund[7], H. Wei[10], F. Plaschke[3], B. J. Anderson[11], G. Le[7], T. E. Moore[7], B. L. Giles[7], W. R. Paterson[7], C. J. Pollock[7], J. C. Dorelli[7], L. A. Avanov[7], Y. Saito[12], B. Lavraud[13], S. A. Fuselier[9], B. H. Mauk[11], I. J. Cohen[11], and J. F. Fennell[1]

[1]Laboratoire de Physique des Plasmas, UMR7648, CNRS, Ecole Polytechnique, UPMC Univ Paris 06, Univ. Paris-Sud, Observatoire de Paris, Paris, France, [2]Space Sciences Department, The Aerospace Corporation, El Segundo, CA, USA, [3]Space Research Institute, Austrian Academy of Sciences, Graz, Austria, [4]Swedish Institute of Space Physics, Uppsala, Sweden, [5]Department of Physics and Space Science Center, University of New Hampshire, Durham, NH, USA, [6]Laboratory for Atmospheric and Space Physics, University of Colorado Boulder, Boulder, CO, USA, [7]NASA Goddard Space Flight Center, Greenbelt, MD, USA, [8]Royal Institute of Technology, Stockholm, Sweden, [9]Southwest Research Institute, San Antonio, TX, USA, [10]Institute of Geophysics and Planetary Physics, University of California, Los Angeles, CA, USA, [11]Applied Physics Laboratory, The Johns Hopkins University, Laurel, MD, USA, [12]Institute for Space and Astronautical Science, Sagamihara, Japan, [13]Institut de Recherche en Astrophysique et Planétologie, CNRS UMR5277/Université Paul Sabatier, Toulouse, France

Abstract Mirror mode waves are ubiquitous in the Earth's magnetosheath, in particular behind the quasi-perpendicular shock. Embedded in these nonlinear structures, intense lion roars are often observed. Lion roars are characterized by whistler wave packets at a frequency ~100 Hz, which are thought to be generated in the magnetic field minima. In this study, we make use of the high time resolution instruments on board the Magnetospheric MultiScale mission to investigate these waves and the associated electron dynamics in the quasi-perpendicular magnetosheath on 22 January 2016. We show that despite a core electron parallel anisotropy, lion roars can be generated locally in the range $0.05–0.2f_{ce}$ by the perpendicular anisotropy of electrons in a particular energy range. We also show that intense lion roars can be observed up to higher frequencies due to the sharp nonlinear peaks of the signal, which appear as sharp spikes in the dynamic spectra. As a result, a high sampling rate is needed to estimate correctly their amplitude, and the latter might have been underestimated in previous studies using lower time resolution instruments. We also present for the first-time 3-D high time resolution electron velocity distribution functions in mirror modes. We demonstrate that the dynamics of electrons trapped in the mirror mode structures are consistent with the Kivelson and Southwood (1996) model. However, these electrons can also interact with the embedded lion roars: first signatures of electron quasi-linear pitch angle diffusion and possible signatures of nonlinear interaction with high-amplitude wave packets are presented. These processes can lead to electron untrapping from mirror modes.

1. Introduction

The Earth's magnetosheath constitutes the interface between the incoming solar wind and the standing magnetosphere. It forms as the plasma is decelerated and heated at the terrestrial bow shock and flows along the frontier of Earth's magnetosphere, that is, the magnetopause.

The magnetosheath is usually divided into two distinct regions: the quasi-parallel magnetosheath located downstream of the quasi-parallel shock, that is, where the angle θ_{Bn} between the shock normal and the

upstream interplanetary magnetic field is less than 45°, and the quasi-perpendicular magnetosheath where $\theta_{Bn} > 45°$. Due to the plasma flowing along the magnetopause, a high velocity shear is observed in the magnetosheath, which is usually characterized by enhanced levels of turbulence (Zimbardo et al., 2010), which can be affected by the numerous wave modes and coherent structures observed (see, e.g., Bale et al., 2009; Breuillard et al., 2016).

The pileup of plasma in front of the magnetopause generates an ion perpendicular temperature anisotropy $T_{\perp i} > T_{\|i}$ ($\|$ and $\perp$ to the background magnetic field) (Sckopke et al., 1983), causing various fluid and kinetic instabilities that lead to the generation of a rich variety of waves (ion cyclotron waves, mirror modes, whistler waves, etc.) and coherent structures that are commonly observed in the magnetosheath (see, e.g., Huang et al., 2016; Huang, Sahraoui, et al., 2017; Maksimovic et al., 2001; Masood et al., 2006; Schwartz, Burgess, & Moses, 1996; Soucek & Escoubet, 2011) . Downstream of the quasi-perpendicular low-β shock, a dominance of ion cyclotron waves (left-hand polarized waves at frequencies just below the ion cyclotron frequency f_{c_i}) with amplitudes of about 3 nT is found, whereas mirror waves are mostly observed downstream of the quasi-perpendicular high-β shock (Czaykowska et al., 2001).

Close to the magnetopause, the mechanism of field line draping also generates an important ion temperature anisotropy causing various waves to grow. Due to the pileup of plasma along the magnetopause, high β_i (typically above 3) are usually observed, and mirror modes (zero-frequency waves in the plasma rest frame) dominate the power spectra at MHD and kinetic scales (see, e.g., Alexandrova, Lacombe, & Mangeney, 2008; Huang, Hadid, et al., 2017). The mirror mode is a compressive ($\delta B_{\|} \gg \delta B_{\perp}$) slow mode with $\vec{k} \perp \vec{B}_0$ and it is linearly polarized with antiphase variations in the density and magnetic field magnitude (Shevyrev et al., 2006).

Embedded in the mirror modes, intense bursts of electromagnetic waves with a center frequency of ~100 Hz are frequently observed in the magnetosheath. These emissions were first recorded on OGO-5 and called "lion roars" (Smith, Holzer, & Russell, 1969; Smith and Tsurutani, 1976) and are a characteristic feature of the wave activity in the magnetosheath, although they can also be observed in the magnetosphere (Baumjohann et al., 2000; Dubinin et al., 2007). Smith and Tsurutani (1976) identified lion roars as whistler mode (right-handed circularly polarized) waves propagating at angles ~20° to the background magnetic field, although Baumjohann et al. (1999) found them more field-aligned ($\theta_k \approx 0.2°$). Zhang, Matsumoto, and Kojima (1998) showed that lion roars cover a wide frequency range from 0.02 to 0.75 Ω_e, where Ω_e is the electron gyrofrequency, but a narrow amplitude range (100–200 pT), whereas Baumjohann et al. (1999) found a narrow frequency range (0.05–0.15 Ω_e) but a rather wide amplitude range (0.2–1 nT).

Observations and simulations in mirror modes showed that lion roars are generated by the cyclotron resonant instability in the magnetosheath plasma under conditions of perpendicular electron temperature anisotropy $T_{e\perp} > T_{e||}$ (see, e.g., Ahmadi, Germaschewski, & Raeder, 2016; Lee, Wu, & Price, 1987; Thorne & Tsurutani, 1981). In fact, in the magnetic field troughs the plasma density increases and the characteristic energy of resonant particles E_r may drop down to values comparable to the thermal electron energy (Thorne & Tsurutani, 1981), and so one may expect a significant increase in the number density of resonant electrons and thus a growth of whistler waves. Masood et al. (2006) also made use of Cluster observation electron distributions to determine the lion roar generation mechanism and concluded that most of the lion roars must have been generated remotely, that is, outside the trapping mirror mode, and hence can travel through mirror modes.

The dynamics of particles within large-amplitude mirror mode waves were studied notably by Kivelson and Southwood (1996) using a theoretical model and observations, where they have shown that there is a critical pitch angle $\alpha_c = \sin^{-1}(\sqrt{|B|/|B|_{\max}})$ for particle trapping (named "resonant" particles therein). Namely, a particle with $\alpha_c \leq \alpha \leq 180 - \alpha_c$ becomes trapped inside the magnetic troughs of the mirror structure and as the mirror wave grows, they gain energy by Fermi acceleration (i.e., nonadiabatically). It was further proposed that to saturate the growth and to attain marginal stability, the trapped population at perpendicular pitch angles lose energy by Fermi deceleration. As a result, particles with α close to 90° are cooled, whereas particle with a pitch angle just greater (less) than α_c ($180 - \alpha_c$) are heated. The heating process is more efficient as the energy of particles is increasing, whereas the cooling process is more efficient when energy is decreasing, as seen on Figure 7c from Kivelson and Southwood (1996). In this picture, some untrapped particles, namely, particles with α just less (greater) than α_c ($180 - \alpha_c$), are also affected by the cooling.

Several studies verified this behavior using ion distributions (Leckband et al., 1995; Soucek & Escoubet, 2011), but to our knowledge, the electron pitch angle distributions inside mirror modes where shown only in

Chisham et al. (1998). Using Active Magnetospheric Particle Tracer Explorer (AMPTE) - UK Subsatellite (UKS) observations, they showed a "cooling" of the electrons with pitch angles close to 90° in the field troughs, and a "heating" of the electrons with pitch angles just greater than a trapping pitch angle (~65°), in agreement with Kivelson and Southwood (1996). However, the authors did not consider the presence of whistler waves in the mirror modes that can interact with electrons through resonant wave-particle interaction.

In the frame of the quasi-linear theory, the interaction between a low-amplitude whistler wave and resonant electrons (i.e., these whose thermal speed is close to the field-aligned phase speed of the wave) results in stochastic diffusion of resonant electron pitch angles and energy (see, e.g., Kennel, 1966; Kennel & Petschek, 1966)). For a sufficiently large-amplitude (nonlinear) wave, the fundamental mode of wave-particle interaction can switch from being stochastic to being deterministic; that is, the pitch angle of the particle varies in a well-defined manner (see, e.g., Albert, 2002; Bortnik, Thorne, & Inan, 2008; Inan, 1987; Inan, Bell, & Helliwell, 1978). If the amplitude is sufficiently high, whistlers can meet a condition where wave forces roughly balance adiabatic forces, resulting in the phase trapping of a small number of particles that undergo a gyrotropic motion along the wave direction (see, e.g., Bortnik, Thorne, & Inan, 2008; Dubinin et al., 2007). To our knowledge, signatures of quasi-linear and nonlinear interaction with whistlers have not been observed in electron distributions inside mirror modes in the magnetosheath yet, due to instrumental limitations.

In this study we take advantage of the high-resolution instruments on board MMS to study lion roars in Earth's magnetosheath and their impact on electron dynamics. The measurements are sampled at an unprecedented rate of 33.3 Hz for electron velocity distribution functions by the Fast Plasma Investigation (Pollock et al., 2016) instrument. The electric field and spacecraft potential are measured at a sampling frequency of 8,92 Hz by Axial Double Probe (Ergun et al., 2016) and Spin Double Probe (Lindqvist et al., 2016) instruments. Low- and high-frequency magnetic field measurements are sampled at a rate of 128 and 8,192 Hz by the fluxgate magnetometer (Russell et al., 2016) and the search coil magnetometer (Le Contel et al., 2016) instruments, respectively. The used snapshot of burst-type data with a length of 50 s was collected in the quasi-perpendicular magnetosheath by the MMS3 spacecraft on 22 January 2016 at 00:19:16 UT. During this time interval the magnetosheath is rather stable (e.g., peaks of the mirror modes are rather steady and the plasma is not very turbulent and does not include kinetic-scale nonlinear structures), which makes it convenient to study mirror modes and lion roars.

In section 2, we describe the properties of the lion roars observed during the considered event. Then, in section 3, we investigate their nonlinear nature by comparing with simulations of linear growth. In section 4, we study their impact on electron dynamics, using notably for the first-time high-resolution 3-D electron velocity distribution functions. Finally, the discussion and conclusions are presented in section 5.

2. The Properties of the Linear Lion Roars

In this section we study the properties of the lion roars observed during the selected event, using FluxGate Magnetometer and Search-Coil Magnetometer, and Electric field Double Probes (EDP) burst waveform data. Figure 1 presents a detailed polarization analysis in the frequency range [10–2,000] Hz using wavelet (Morlet) analysis: Figures 1a and 1b show the total magnetic and electric dynamic spectra; Figures 1c and 1d display the ellipticity and the angle θ_k between the background magnetic field and the wave vector; Figures 1e and 1f show the degree of polarization and the planarity; and finally, Figures 1g and 1h present the wave phase velocity (defined by $|E|/|B|$) and the Poynting flux component along the background magnetic field ($S_z/|S|$).

In this figure, intense (up to ~1.7 nT, see in Figure 3) electromagnetic wave packets of ~1–2 s are observed in the frequency range [~35–280] Hz (i.e., [~0.05–0.4] f_{ce} which are shown as the dotted and dashed lines, respectively). They are nearly monochromatic right-handed circularly polarized (ellipticity ~1), with a high degree of polarization >0.9. They propagate close to the background magnetic field ($|\theta_k| \leq 20°$), at a phase velocity $v_{ph} \approx 10^6$ m/s, in the direction opposite to the magnetic field since the Poynting vector component parallel to B_0 (S_z) is negative (Figure 1h). Thus, these fluctuations fill all the criteria of magnetosheath lion roars (see Baumjohann et al., 1999; Smith, Holzer, & Russell, 1969; Smith & Tsurutani, 1976), except that some of the lion roars observed here are more oblique ($\theta_k \approx 30–50°$, consistent with Maksimovic et a., 2001).

The frequency range is thus consistent with a local generation, but surprisingly, when computing the moments, we obtain a parallel anisotropy ($T_{e\perp}/T_{e||} < 1$). This seems incompatible with local whistler wave growth (see Thorne & Tsurutani, 1981) and would be rather in favor of remotely generated lion roars (i.e., outside

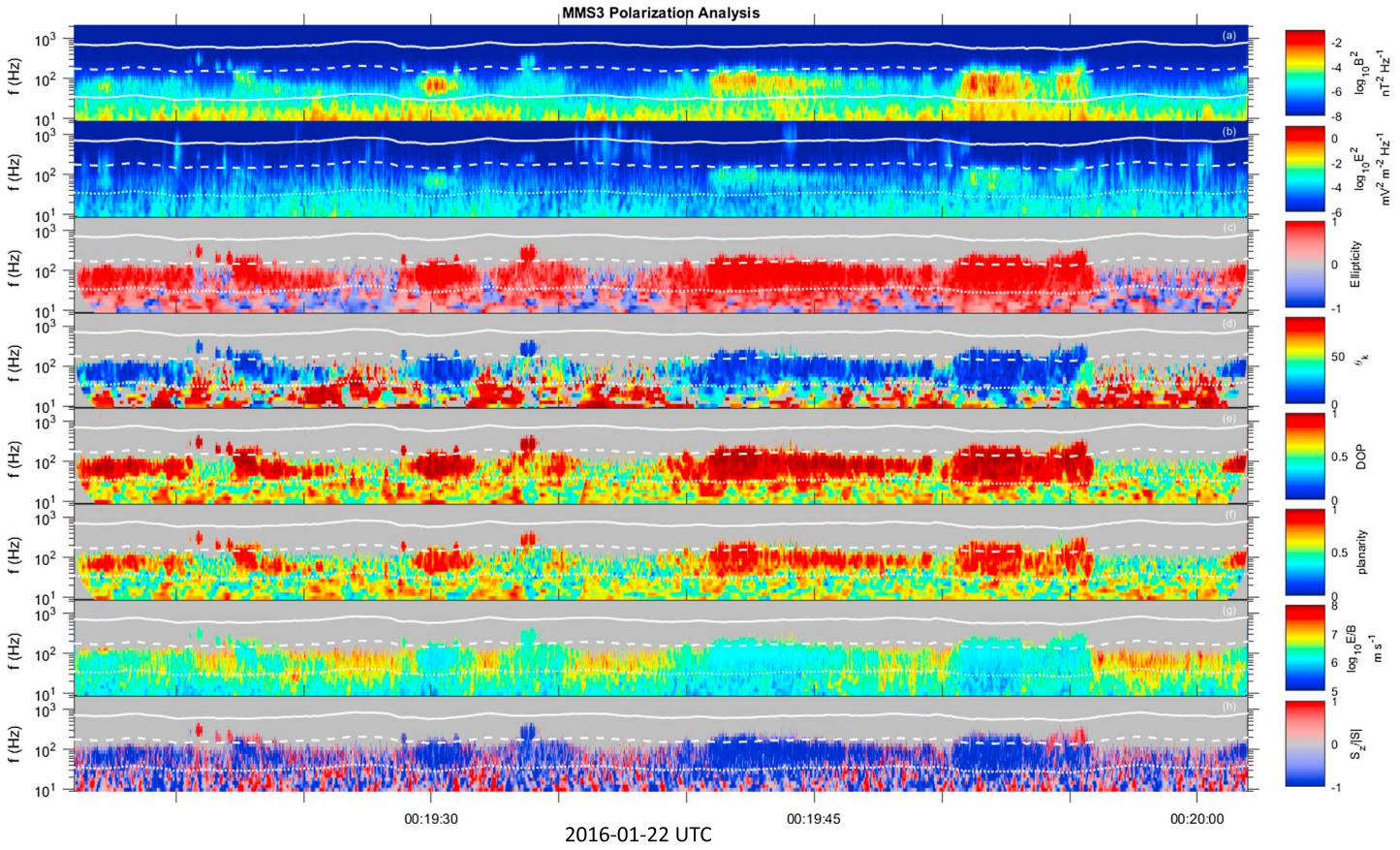

Figure 1. Detailed polarization analysis of the considered event in the frequency range [10–2,000] Hz: (a and b) the total magnetic and electric dynamic spectra; (c and d) the ellipticity and the angle θ_k between the background magnetic field and the wave vector; (e and f) show the degree of polarization and the planarity; and finally (g and h) the wave phase velocity (defined by $|E|/|B|$) and the Poynting flux component along the background magnetic field ($S_z/|S|$). Solid, dashed, and dotted white lines represent f_{ce}, $0.2f_{ce}$ and $0.04f_{ce}$, respectively.

the considered mirror mode), as stated in Masood et al. (2006). However, we will see below that the anisotropy depends considerably on the considered energy range and can be perpendicular ($T_{e\perp}/T_{e||} > 1$) for the energy ranges that resonate with whistler instability. This topic is discussed in section 4, where electron distribution functions are presented. Note that some wave packets have an inverse Poynting vector (in red) but have a different center frequency ($f > 0.2f_{ce}$) and are less intense, so they may come from another source, outside the considered mirror modes.

In order to confirm the observations of these waves, we compute the linear wave dispersion using the Waves in Homogeneous, Anisotropic Multicomponent Plasmas (WHAMP) solver (Rönnmark, 1982) for the most intense lion roar (00:19:51–00:19:54 UT) presented in Figure 1. The dispersion relation is obtained using the local plasma parameters (based on FGM and FPI measurements for ~100 eV electrons shown in Figure 5 below, but which are also typical for magnetosheath) and considering 2 different Maxwellian populations (ions and electrons): $|B| = 20$ nT, $n_e = n_i = 30$ cm^{-3}, $T_e = 100$ eV, and $T_i = 1,000$ eV. Ions are considered isotropic, and electrons present a perpendicular anisotropy $A_e = T_{e\perp}/T_{e||} = 1.25$, as it can be seen in Figures 5g and 5h.

The simulation, presented in Figure 2, shows a large linear wave growth (~$0.025\ \mathrm{Im}(\omega)/\Omega_e$) of parallel whistlers in the frequency range $0.05 - 0.2f_{ce}$, that is, [35–140] Hz. This result is in good agreement with the observed frequency range of most wave packets in Figure 1. However, in this figure, even though most of the wave packets are well constrained by the classical upper limit $0.2f_{ce}$ (Baumjohann et al., 1999), the most intense wave packets seem to reach frequencies above this limit. For instance, the most intense wave packet (00:51–00:54 UT) reaches frequencies ~280 Hz, that is, ~ $0.4f_{ce}$, which cannot be explained by the linear wave growth. We point out that these fluctuations are seen well above the noise level (not shown). The nature of these fluctuations is discussed in the next section.

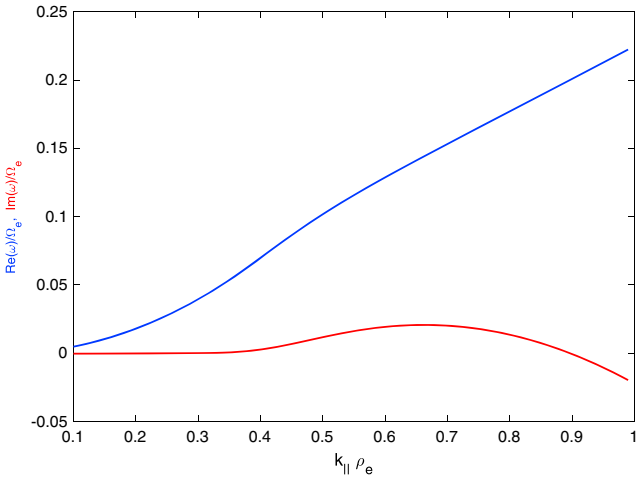

Figure 2. WHAMP simulation of whistler waves generation using the local plasma parameters, considering two different Maxwellian populations (ions and electrons): $|B| = 20$ nT, $n_e = n_i = 30$ cm^{-3}, $T_e = 100$ eV, and $T_i = 1,000$ eV (temperatures are derived from FPI and correspond to typical magnetosheath parameters). Ions are considered isotropic and electrons present a perpendicular anisotropy $A_e = T_{e\perp}/T_{e||} = 1.25$, as it can be seen in Figures 5g and 5h. Real and imaginary (growth rate) parts of the frequency, normalized to the electron gyrofrequency (Ω_e), are shown in blue and red, respectively. The parallel wave vector $k_{||}$ is normalized to the electron gyroradius ρ_e.

3. The Nonlinear Characteristics of Lion Roars

To unveil the nature of these high-frequency fluctuations, we first test that the linear whistlers are not Doppler shifted in the spacecraft frame. This Doppler-shifted frequency is expressed as $\omega_{sc} = \omega_{pl} - \vec{k} \cdot \vec{v}$, where ω_{pl} is the frequency in the plasma frame, $\vec{k}$ is the wave vector, and $\vec{v}$ is the bulk velocity vector with respect to the spacecraft. Yet $\vec{k}$ is quasi-parallel to the magnetic field ($\theta_k \approx 10°$), in contrast to $\vec{v}$ which is almost perpendicular ($\theta_{vB} \approx 85°$ at 00:51–00:54 UT, not shown). Thus, $\vec{k} \cdot \vec{v} \approx 0$ and the measured ω_{sc} should be equal to ω_{pl}, derived from WHAMP simulations described in the previous section.

Then, we show that these fluctuations are wave packets coherent with the nonlinear evolution of whistlers, and not weak turbulence (i.e., an incoherent energy cascade toward higher frequencies). To do so, in Figure 3 we compute the dynamic spectrum (Figure 3c) of the most intense lion roar considered in the previous section (00:51–00:54 UT) and study the magnetic waveform in the linear whistler bandwidth (Figure 3b) and in the additional bandwidth (Figure 3a). This is achieved simply by rotating the waveforms in the field-aligned coordinate (FAC) system (i.e., the first two components $B_{\perp 1}, B_{\perp 2}$ are perpendicular to the mean magnetic field $\vec{B_0}$, and the third component $B_{||}$ is parallel to $\vec{B_0}$) and filter them in the appropriate bandwidth ([50–100] and [150–220] Hz, respectively), using an infinite pulse filter (see, e.g., Breuillard et al., 2016).

It is clear from Figure 3a that the perpendicular components are coherent (i.e., structured) wave packets, modulated by the lower-frequency linear whistler waves observed in Figure 3b. Thus, this additional bandwidth is a purely nonlinear effect of the high-amplitude signal peaks of the coherent linear whistlers: as the amplitude of the signal grows, the peaks of the signal become narrower; thus, the frequency of the fluctuations increases at these peaks. In a time-frequency spectrum, this phenomenon will appear as "spikes" at the signal peaks. This is seen in Figure 3c, where the high-frequency bandwidth ($>0.2f_{ce}$) is composed of spectral spikes of the order of a few milliseconds, whose amplitudes vary with the lower-frequency wave packets amplitude B_w, whenever $B_w > 0.5$ nT. We note here that this nonlinear effect does not appear in this event for $B_w < 0.5$ nT (not shown). Thus, in this event we define linear lion roars the wave packets for which $B_w < 0.5$ and nonlinear whistlers those for which $B_w > 0.5$.

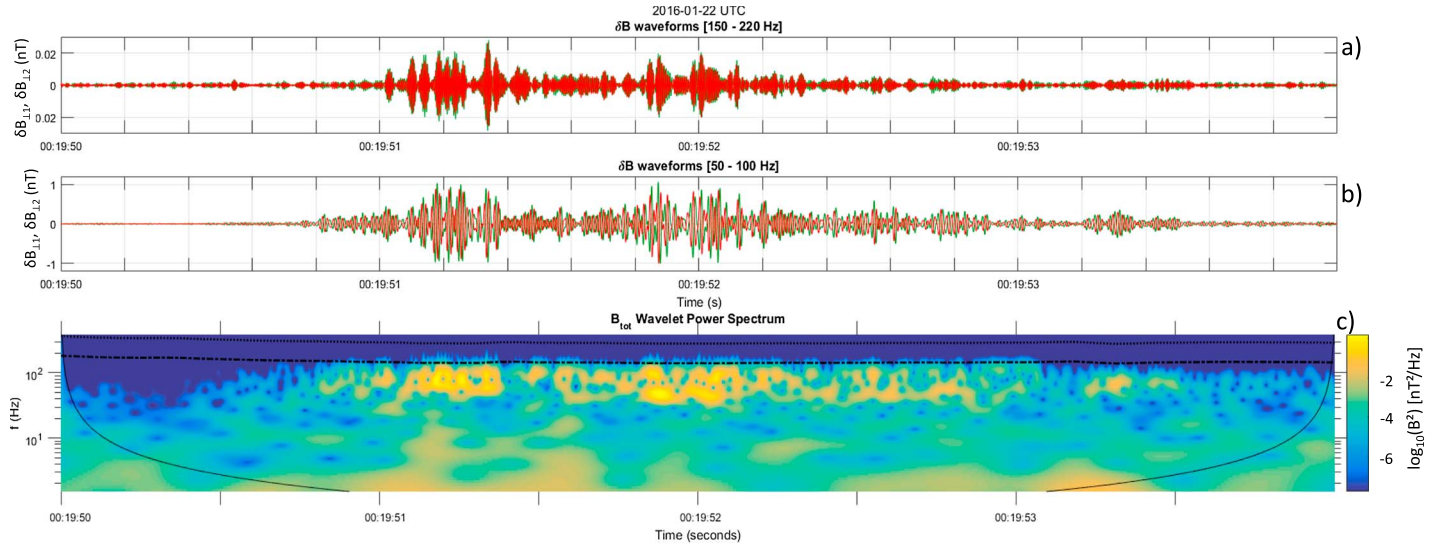

Figure 3. Detailed magnetic waveforms observed for the most intense lion roar (00:19:51–00:19:53) in the field-aligned coordinates (FAC) for the two considered frequency ranges: (a) [150–220] Hz, (b) [50–100] Hz. (c) The dynamic spectrum of the wave packet, with the linear whistlers constrained by $0.2f_{ce}$ (dash-dotted black line) and the nonlinear whistlers appear as spikes above this limit. The dotted black line represents $0.5f_{ce}$.

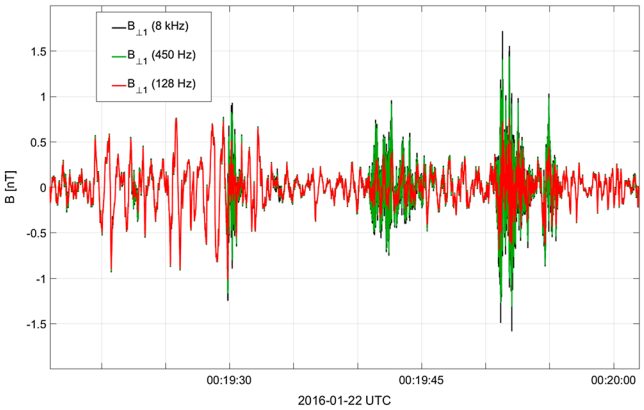

Figure 4. Waveform of the first component of the perpendicular fluctuations ($B_{\perp 1}$, in the FAC system) measured by SCM for the whole event (00:19:16–00:20:02 UT). Signals at different sampling rates are shown using different colors: 8 kHz signal is in black (original MMS sampling rate), 180 Hz downsampled signal is in green (similar to Cluster sampling rate) and 128 Hz downsampled signal is in red (similar to Equator-S sampling rate).

As a result, a high sampling rate of magnetic measurements is required to resolve correctly these high-amplitude signal peaks (see Zhang, Matsumoto, & Kojima, 1998). In fact, if the signal is undersampled by the instrument and the discrete samples do not match the peaks, then the amplitude of the signal can be largely underestimated by the discrete measurements. To illustrate this statement, we show in Figure 4 the high-frequency perpendicular fluctuations (in the FAC system), collected by SCM in burst mode (sampled at 8,192 Hz) during the whole event (00:19:16–00:20:02 UT). Then, we numerically downsample this signal to values used on Cluster and Equator-S missions for comparison, since data from these missions have been used previously to study statistically the amplitudes of lion roars (Baumjohann et al., 1999; Dubinin et al., 2007). To avoid aliasing, two steps are considered: first, we filter the signal to 180 Hz (similarly to STAFF on board Cluster (see Cornilleau-Wehrlin et al., 1997)) and 64 Hz (similarly to Equator-S magnetometer; see Fornacon et al., 1999), and then the signal is numerically downsampled to 450 and 128 Hz, respectively.

Using the 128 Hz sampling rate, we see that the amplitude is very badly estimated for all wave packets, even low-amplitude (linear) lion roars ($B_w < 0.5$ nT). For high-amplitude lion roars, the amplitude can be underestimated by 2 orders of magnitude compared to the 8,192 Hz sampling rate. The 180 Hz sampling rate, on the other hand, provides a good estimation for low-amplitude lion roars ($B_w < 0.5$ nT), but is less accurate for high-amplitude (nonlinear) lion roars ($B_w \geq 0.5$ nT). For instance, the amplitude of the most intense wave packet ($B_w \sim 1.7$ nT at 00:52 UT) is underestimated by the 180 Hz sampling rate by ~20%. Therefore, the amplitude of lion roars may have been underestimated by previous studies using lower time resolution instruments. This can have a significant impact on electron dynamics, as stated in the introduction (see also Dubinin et al., 2007).

4. The Effects of Mirror Modes and Lion Roars on Electron Dynamics

In this section we take advantage of the unprecedented time resolution of the Fabry-Perot interferometer (FPI) instrument to determine for the first time the effects of mirror modes and embedded lion roars on 3-D electron velocity distributions. The sampling rate of FPI (32 Hz for electrons in burst mode) indeed allows to resolve velocity distributions at ion scales in the magnetosheath for the first time.

These electron distributions are presented in Figure 5 for the whole time interval considered (00:19:16–00:20:02 UT). Figure 5a displays the total magnetic field $|B|$ and the electron density n_e measured by FGM and FPI instruments, respectively. $|B|$ and n_e fluctuations are clearly anticorrelated, which is characteristic of mirror mode waves, with a period of ~5–10 s (i.e., 0.2–0.1 Hz). The bottom of the magnetic "bottles" are thus defined by the $|B|$ minima and the n_e maxima, where the lion roars are observed (i.e., the fluctuations shown in Figure 5b).

This is explained by the fact that when $|B|$ is at minimum, then the resonant energy to generate whistlers is decreased and closer to the thermal energy, and as n_e is at a maximum, the number of resonant particles greatly increases (Thorne & Tsurutani, 1981). As a result, the amplitude of the lion roars should increase as the difference between n_e and $|B|$ increases (i.e., close to the bottom of the mirror mode, where whistlers are generated), which can be seen in Figures 5a and 5b.

The electron velocity distributions inferred from FPI are shown in Figures 5c to 5i. In Figures 5d to 5i, where pitch angle distributions are shown, we superimpose the critical pitch angle α_c and $180 - \alpha_c$ (black solid lines) described in the introduction ($B_{\max} = 31$ nT is defined here as the maximum value during the considered time interval), to compare the electron dynamics due to mirror modes and the embedded lion roars.

Figure 5c shows the omnidirectional flux of electrons from 10 eV to 10 keV, where the fluxes are shown to be very steady as the magnetosheath is very quiet during this time period. Only some local cooling of very high energy electrons (1–10 keV) can be observed when high-amplitude lion roars are observed. The cooling of parallel and mostly antiparallel high-energy electrons where intense whistlers are observed is confirmed in Figure 5i, for example, at 00:19:34 UT.

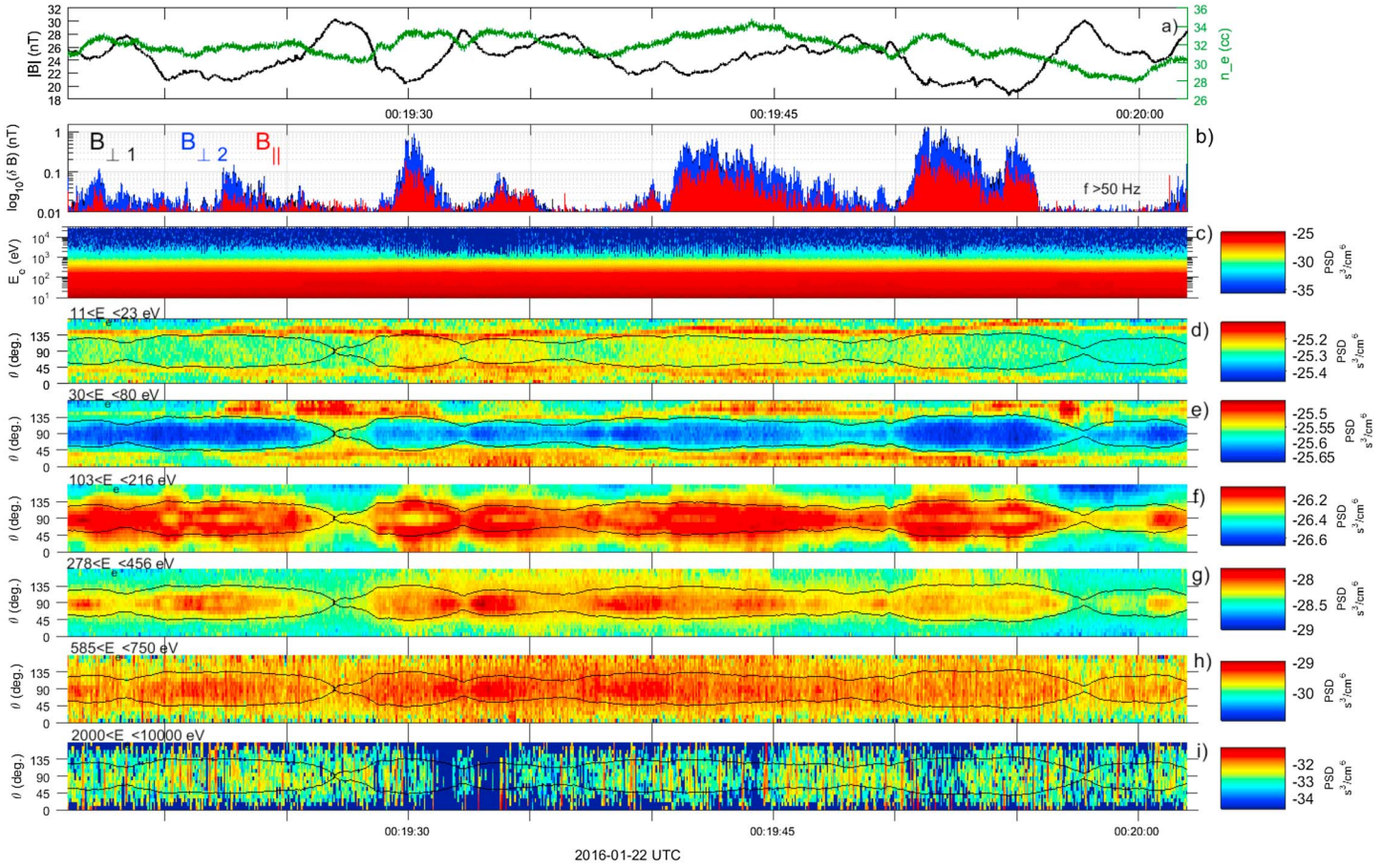

Figure 5. Correlation between whistler waves and electron velocity distribution functions: (a) the $|B|$ and n_e fluctuations and (b) the whistler magnetic waveforms in FAC. (c) The omnidirectional flux as a function of time is presented for the whole FPI energy range [10–10,000] eV. (d to i) The electron pitch angle distributions during the whole event for different energy ranges.

For core electrons (11–23 eV, Figure 5d), as mentioned above, the anisotropy is observed to be mostly parallel, which is why we find a parallel anisotropy when computing the moments from FPI. This parallel anisotropy is due to parallel and antiparallel electron beams ($\alpha \approx 45, 135°$). The poor correlation between core electron pitch angles and α_c suggests that these electrons are too cold to interact with the mirror modes.

In contrast, for electrons in the range [30–80 eV], even if the parallel and antiparallel beams are still dominant (meaning that most of the particles at these energies are not trapped in the mirror modes), the correlation between the pitch angle distribution and α_c is evident. A large cooling of electrons that are deeply trapped (i.e., with $\alpha \approx 90°$) is observed, whereas there is a slight heating of shallowly trapped electrons (i.e., with α slightly greater than α_c and slightly less than $180 - \alpha_c$), as described in Figure 7c (for low energy particles) from Kivelson and Southwood (1996). We note here that the depth of the trapping appears to increase with decreasing (increasing) α_c ($180 - \alpha_c$), that is, with the depth of the magnetic bottle.

At higher energies, in the range [103–216] eV, the correlation between the pitch angle distributions and α_c is also evident. Most of the electrons are shallowly trapped in the mirror modes, and the heating of shallowly trapped electrons this time appears more effective than the cooling of deeply trapped particles, which is also expected from the Kivelson and Southwood (1996) model for higher energies (i.e., larger velocities see Figure 7c therein). However, according to this model, untrapped particles should be cooled as well close to α_c, whereas in Figure 5f we observe a significant isotropic heating of untrapped particles, that is, up to very small (large) pitch angles, close to 0° (180°). This significant heating of untrapped particles seems well correlated with the presence of whistler waves (see Figure 5b).

In the energy range [216–356] eV, again most of the electrons are trapped in the mirror modes, and the heating is even broader in energy for shallowly trapped electrons, whereas the cooling of deeply trapped electrons

is narrower. This is again expected from the Kivelson and Southwood (1996) model for even higher energies (see again Figure 7c therein). However, in contrast with the latter model, a significant heating of untrapped electrons is again observed but this time only in the direction antiparallel to the magnetic field (180°). This anisotropic heating seems correlated with high-amplitude lion roars ($B_w \geq 0.5$ nT).

At the largest considered energies, the distributions tend to be more isotropic, which means that the electrons are less affected by the mirror modes structures. However, in the energy range [456–585] eV, a perpendicular anisotropy is clearly present due to the heating of the deeply trapped particles. The observed perpendicular anisotropy in the energy range [216–585] eV can thus be responsible for the generation of whistler waves. In the highest energy range (Figure 5i), the distribution is slightly noisy, but a cooling of energetic electrons is observed (see also in Figure 5a) in the presence of whistler waves (e.g., at 00:19:34 UT).

The results shown here are discussed in the following section.

5. Discussion and Conclusions

In this study, we make use of the unprecedented high temporal resolution of particle and fields measurements on board the MMS mission to investigate the properties of lion roars, that is, intense whistler wave packets typically embedded in mirror modes, and their impact on electron dynamics. In this section, we discuss the results obtained and their implications for future work.

We first study the waveforms of the intense wave packets observed. The wave polarization analysis is consistent with whistler modes propagating close to the background magnetic field ($|\theta_k| \leq 20°$) in the frequency range $0.05–0.4f_{ce}$. The waves are slightly more oblique than in Baumjohann et al. (1999), but consistent with other studies (e.g., Masood et al., 2006). Some whistlers are also observed more oblique $30° \leq \theta_k \leq 50°$, which is consistent with results of Maksimovic et al. (2001).

Using the WHAMP solver, we also show that the observed waves in the range [35–140] Hz (i.e., $0.05–0.2f_{ce}$) can be generated locally by the perpendicular temperature anisotropy of ~100 eV electrons, which is due to compression in the mirror modes. While computing the moments (integrated over all energy channels) gives a parallel anisotropy (see Figures 5d and 5e), a perpendicular anisotropy of electrons in the energy range [103–585] eV is seen later on in Figures 5g and 5h. Thus, while some lion roars can appear as remotely generated from the plasma temperature (Masood et al., 2006), it is necessary to carefully check the different energies to make a firm statement.

However, intense wave packets ($B_w > 0.5$ nT) are also observed up to $0.4f_{ce}$, which cannot be explained by a temperature anisotropy. Thus, by analyzing the waveforms in the different frequency ranges (see Figure 3), we show that the waves observed in the range [150–220 Hz] are coherent wave packets modulated by the whistlers generated by temperature anisotropy. As a result, as the whistlers grow, the nonlinear peaks of the wave packets become narrower and appear as sharp spikes in the dynamic spectrum that can reach higher frequencies (here $\sim 0.4f_{ce}$).

We then deduce that a high sampling rate is required to estimate correctly the amplitude of lion roars, as the whistlers can reach 1.7 nT in our case, which corresponds here to a frequency of ~280 Hz. In fact, we show that if the signal is undersampled, some peaks are not picked up by the measurements and the amplitude is underestimated. Hence, the measurement of their usual amplitude (usually 0.1–0.2 nT) might have been limited by the sampling rate of instruments (e.g., 128 Hz on Equator-S) or the antialiasing filter applied (e.g., 180 Hz on Cluster) on previous missions (see Figure 4). Thus, a statistical study of lion roars amplitude by high time resolution instruments such as SCM on board MMS would be interesting to confirm this hypothesis and is left for future work.

Such underestimation of the amplitude may have important consequences on the impact of these waves on electron dynamics. Therefore, in the last section we present for the first-time high-resolution 3-D electron velocity distributions in mirror modes, using FPI sampling rate of 32 Hz. First, we identify mirror mode structures (with a 5–10 s period) by the antiphase variations of $|B|$ and n_e, and the lion roars are clearly observed in the trough of the magnetic bottles. Then, we show that the core (or bulk) electrons (10–30 eV) do not interact with the mirror mode structures (they have a quasi-isotropic pitch angle distribution; that is, they do not exchange energy with the structures), but they present electron beams at $\alpha \approx 45°$ (135°). However, the origin of these electron beams is unclear and beyond the scope of this study.

Table 1
Estimated Energies for the Landau ($m = 0$) and the Cyclotron ($m = \pm 1$) Resonances Derived From Equation (1), Using $B_0 = 25$ nT and $n_e = 30$ cm^{-3}

Wave parameters	$E_{r,\text{Landau}}$ (eV)	$E_{r,\text{cyclotron}}$ (keV)[a]
$\omega/\Omega_e = 0.05, \theta = 0°$	35	10, 10
$\omega/\Omega_e = 0.15, \theta = 15°$	95	5, 3
$\omega/\Omega_e = 0.25, \theta = 50°$	170	4.3, 1.5

[a]The first value corresponds to $m = 1$ and the second $m = -1$.

In the middle energy range [~30–585] eV, electrons that are trapped in the mirror modes (i.e., particles with α closer to 90° than α_c) interact with the mirror modes, as expected from the so-called "resonant" particles (Kivelson & Southwood, 1996; Southwood & Kivelson, 1993). At lower energies (e.g., 30–80 eV), the cooling (or Fermi deceleration) is more effective (proportional to the electron energy) for deeply trapped electrons than the heating for shallowly trapped electrons (see the definitions in Kivelson & Southwood, 1996). As a result, in this energy range the nonresonant particles (with a large parallel velocity) dominate and the distribution is highly anisotropic with a peak at 30° and a deep trough at 90°. The trough appears to be proportional to the depth of the magnetic bottle.

As expected from Kivelson and Southwood (1996), as the energy increases, the cooling of deeply trapped electrons is weakening whereas the heating of shallowly trapped electrons is strengthening and broadening toward larger α (i.e., closer to 90°, see Figure 7c in Kivelson & Southwood, 1996). As a result, in the energy range [103–216] eV (see Figure 5f), the peaks of the distribution are seen close to 60° (i.e., α_c) with a slight trough at 90°, as also observed by Chisham et al. (1998). Moreover, in the range [216–356] eV (see Figure 5g) the peaks are seen more perpendicular (75°) and in some cases a large perpendicular anisotropy is observed (e.g., at 00:19:38–00:19:45 UT).

This large perpendicular anisotropy is also observed at higher energies (456–585 eV), where some electrons are deeply trapped, but the heating of shallowly trapped electrons and the cooling of deeply trapped ones cannot be distinguished anymore. Therefore, the perpendicular anisotropy in the energy range [~100–500] eV may be responsible for the generation of the lion roars, as demonstrated in Figure 2 where we observe a positive growth rate at $0.05–0.2 f_{ce}$ using an anisotropic electron population ($A_e = 1.25$) with a mean energy of 100 eV.

Consequently, electrons will interact not only with mirror mode structures but also with the locally generated whistlers. To verify such statement, we calculate the energy range for which the electrons can resonate with the whistler wave. For obliquely propagating waves, the resonant energies for electrons can be derived, in the frame of the quasi-linear theory, from the following equation (see, e.g., Lengyel-Frey et al., 1994):

$$E_{r,e} = \frac{B_0^2}{2\mu_0 n_e} \frac{\Omega_e}{\omega \cos^2\theta} \left(\cos\theta - \frac{\omega}{\Omega_e}\right) \left(m + \frac{\omega}{\Omega_e}\right)^2 \quad (1)$$

where B_0 is given in nanoteslas, n_e in cubic centimeters, $E_{r,e}$ in kelvin, and $m = 0, 1, -1$ correspond to the Landau resonance, normal cyclotron resonance, and anomalous cyclotron resonance, respectively.

Using equation (1), we calculate the mean resonant energies considering the linear whistler wave parameters generated in Figure 2, and observed in Figure 1. These values are consigned in Table 1, from minimum (top row) to maximum (bottom row) wave frequency. Table 1 shows that the energy range is [~35–170] eV for Landau resonance and [~1.5–10] keV for cyclotron resonance with the whistler waves. Thus, the Landau resonance energy range corresponds to Figures 5e and 5f and the cyclotron resonance to Figures 5h and 5i. However, this result shows that quasi-linear wave-particle interaction does not cover the [278–750] eV range which corresponds to Figures 5g and 5h.

In Figure 5f, we observe a large heating of untrapped particles (up to 0–180° pitch angles), whereas in the Kivelson and Southwood (1996) model the heating occurs only for shallowly trapped particles and some untrapped particles close to α_c are even cooled (see Figure 7c therein). The electron energy range ([103–216] eV) in this panel belongs to the Landau resonance energies. Since this heating is also isotropic and seems correlated with the presence of whistlers, even at low amplitude (e.g., there is no heating of untrapped particles at 00:19:27 and 00:20:00 UT when no whistlers are observed), this could be a signature of quasi-linear electron pitch angle scattering by whistlers. Indeed, in this process, the particle trajectory through a small

amplitude wave represents a random walk in velocity space and thus a diffusive spread in pitch angle and energy of the particle is observed (see, e.g., Albert, 2001; Inan, 1987; Kennel, 1966; Kennel & Petschek, 1966).

In contrast, in Figure 5g, an anisotropic heating of untrapped particles is observed (mostly in the antiparallel direction). This anisotropic heating cannot be explained by electron pitch angle scattering but appears to be correlated to nonlinear (i.e., high amplitude $B_w \geq 0.1$ nT) whistlers and is in the same direction as the Poynting flux (i.e., the energy direction of propagation): antiparallel to the magnetic field. Thus, this could be a signature of nonlinear interaction with large-amplitude whistlers. Indeed, as stated in section 1, for sufficiently large wave amplitudes the fundamental mode of wave-particle interaction can become deterministic due to the gyrotropic motion of resonant (trapped) electrons along the wave direction (see, e.g., Albert, 2002; Inan, 1987; Inan, Bell, & Helliwell, 1978). This shifts the pitch angle away from 90° (see, e.g., Bortnik, Thorne, & Inan, 2008; Dubinin et al., 2007) and in the direction of the Poynting flux (here 180°, see Figure 1), which is observed in Figure 5g. Since, as stated above, quasi-linear interaction does not cover the energy range shown in this panel, this pitch angle shift may be due to nonlinear processes. However, a detailed study using simulations is needed to firmly determine which process is at work here, which is beyond the scope of this study.

Finally, at higher energies (>456 eV, Figures 5h and 5i), the distributions tend to be more isotropic as they interact less with the mirror mode structures. However, in the energy range [585–750] eV (Figure 5h) a decrease of the perpendicular anisotropy is observed when high-amplitude lion roars are present, and in the energy range [2–10] keV (Figure 5i), a cooling of electrons is also observed, as already seen in Figure 5c. Since these energy ranges correspond to cyclotron resonance energies (see above), these properties can be the signatures of this phenomenon. Nevertheless, this point is out of the scope of this study and is left for future investigation.

To conclude, we summarize our main results as follows:

1) High-amplitude (up to 1.7 nT) lion roars are detected in Earth's magnetosheath by high time resolution instruments onboard the MMS mission.
2) Despite the core electron parallel anisotropy, waves are generated locally in the frequency range $0.05-0.2f_{ce}$ by the perpendicular anisotropy of electrons in the energy range [~100–500] eV.
3) The high-frequency observed ($\sim 0.4f_{ce}$) is due to the sharp nonlinear peaks of the signal that appear as spikes in the dynamic spectrum.
4) A high sampling rate is needed to estimate correctly their amplitude, and the latter might have been underestimated in previous studies using lower time resolution instruments.
5) Pitch angle distributions of electrons trapped in the mirror mode structures are consistent with Kivelson and Southwood (1996) model: deeply (shallowly) trapped electrons are cooled (heated), and the cooling (heating) is weaker (stronger) as the energy increases.
6) Electrons also interact with lion roars: first signatures of electron quasi-linear pitch angle diffusion are presented and possible signatures of nonlinear interaction with high-amplitude wave packets are shown.
7) These two processes can lead to electron untrapping from mirror mode structures.

However, as stated above, these three processes (namely, interaction with mirror modes and quasi-linear and nonlinear whistlers) can occur in the same energy range (here [100–500] eV) and overlap, which makes it difficult to distinguish and estimate their respective effect on electron dynamics. Hence, a detailed study using both high-resolution observations and simulations is required, which should be the topic of future investigation.

Acknowledgments
This work was supported by the CNES grant "Allocations de recherche post-doctorale." The French involvement (SCM) on MMS is supported by CNES and CNRS. All MMS data used are available at https://lasp.colorado.edu/mms/sdc/public/about/browse-wrapper.

References

Ahmadi, N., Germaschewski, K., & Raeder, J. (2016). Effects of electron temperature anisotropy on proton mirror instability evolution. *Journal of Geophysical Research: Space Physics*, *121*, 5350–5365. https://doi.org/10.1002/2016JA022429

Albert, J. M. (2001). Comparison of pitch angle diffusion by turbulent and monochromatic whistler waves. *Journal of Geophysical Research*, *106*(A5), 8477–8482. https://doi.org/10.1029/2000JA000304

Albert, J. M. (2002). Nonlinear interaction of outer zone electrons with VLF waves. *Geophysical Research Letters*, *29*(8), 1275. https://doi.org/10.1029/2001GL013941

Alexandrova, O., Lacombe, C., & Mangeney, A. (2008). Spectra and anisotropy of magnetic fluctuations in the Earth's magnetosheath: Cluster observations. *Annales Geophysicae*, *26*, 3585–3596. https://doi.org/10.5194/angeo-26-3585-2008

Bale, S. D., Kasper, J. C., Howes, G. G., Quataert, E., Salem, C., & Sundkvist, D. (2009). Magnetic fluctuation power near proton temperature anisotropy instability thresholds in the solar wind. *Physical Review Letters*, *103*(21), 211101. https://doi.org/10.1103/PhysRevLett.103.211101

Baumjohann, W., Georgescu, E., Fornacon, K.-H., Auster, H. U., Treumann, R. A., & Haerendel, G. (2000). Magnetospheric lion roars. *Annales Geophysicae*, *18*, 406–410. https://doi.org/10.1007/s00585-000-0406-2

Baumjohann, W., Treumann, R. A., Georgescu, E., Haerendel, G., Fornacon, K.-H., & Auster, U. (1999). Waveform and packet structure of lion roars. *Annales Geophysicae*, *17*, 1528–1534. https://doi.org/10.1007/s00585-999-1528-9

Bortnik, J., Thorne, R. M., & Inan, U. S. (2008). Nonlinear interaction of energetic electrons with large amplitude chorus. *Geophysical Research Letters*, *35*, L21102. https://doi.org/10.1029/2008GL035500

Breuillard, H., Yordanova, E., Vaivads, A., & Alexandrova, O. (2016). The effects of kinetic instabilities on small-scale turbulence in Earth's magnetosheath. *The Astrophysical Journal*, *829*, 54. https://doi.org/10.3847/0004-637X/829/1/54

Chisham, G., Burgess, D., Schwartz, S. J., & Dunlop, M. W. (1998). Observations of electron distributions in magnetosheath mirror mode waves. *Journal of Geophysical Research*, *103*, 26,765–26,774. https://doi.org/10.1029/98JA02620

Cornilleau-Wehrlin, N., Chauveau, P., Louis, S., Meyer, A., Nappa, J. M., Perraut, S., … Louarn, P. (1997). The cluster Spatio-Temporal Analysis of Field Fluctuations (STAFF) experiment. *Space Science Reviews*, *79*, 107–136. https://doi.org/10.1023/A:1004979209565

Czaykowska, A., Bauer, T. M., Treumann, R. A., & Baumjohann, W. (2001). Magnetic field fluctuations across the Earth's bow shock. *Annales Geophysicae*, *19*, 275–287. https://doi.org/10.5194/angeo-19-275-2001

Dubinin, E. M., Maksimovic, M., Cornilleau-Wehrlin, N., Fontaine, D., Travnicek, P., Mangeney, A., … Andre, M. (2007). Coherent whistler emissions in the magnetosphere: Cluster observations. *Annales Geophysicae*, *25*(1), 303–315. https://doi.org/10.5194/angeo-25-303-2007

Ergun, R. E., Tucker, S., Westfall, J., Goodrich, K. A., Malaspina, D. M., Summers, D., … Cully, C. M. (2016). The axial double probe and fields signal processing for the MMS mission. *Space Science Reviews*, *199*(1), 167–188. https://doi.org/10.1007/s11214-014-0115-x

Fornacon, K.-H., Auster, H. U., Georgescu, E., Baumjohann, W., Glassmeier, K.-H., Haerendel, G., … Dunlop, M. (1999). The magnetic field experiment onboard Equator-S and its scientific possibilities. *Annales Geophysicae*, *17*, 1521–1527. https://doi.org/10.1007/s00585-999-1521-3

Huang, S. Y., Hadid, L. Z., Sahraoui, F., Yuan, Z. G., & Deng, X. H. (2017). On the existence of the Kolmogorov inertial range in the terrestrial magnetosheath turbulence. *The Astrophysical Journal Letters*, *836*(1), L10.

Huang, S. Y., Sahraoui, F., Retino, A., Le Contel, O., Yuan, Z. G., Chasapis, A., … Burch, J. L. (2016). MMS observations of ion-scale magnetic island in the magnetosheath turbulent plasma. *Geophysical Research Letters*, *43*, 7850–7858. https://doi.org/10.1002/2016GL070033

Huang, S. Y., Sahraoui, F., Yuan, Z. G., He, J. S., Zhao, J. S., Contel, O. L., … Burch, J. L. (2017). Magnetospheric multiscale observations of electron vortex magnetic hole in the turbulent magnetosheath plasma. *The Astrophysical Journal Letters*, *836*(2), L27.

Inan, U. S. (1987). Gyroresonant pitch angle scattering by coherent and incoherent whistler mode waves in the magnetosphere. *Journal of Geophysical Research*, *92*(A1), 127–142. https://doi.org/10.1029/JA092iA01p00127

Inan, U. S., Bell, T. F., & Helliwell, R. A. (1978). Nonlinear pitch angle scattering of energetic electrons by coherent VLF waves in the magnetosphere. *Journal of Geophysical Research*, *83*(A7), 3235–3253. https://doi.org/10.1029/JA083iA07p03235

Kennel, C. (1966). Low-frequency whistler mode. *Physics of Fluids*, *9*, 2190–2202. https://doi.org/10.1063/1.1761588

Kennel, C. F., & Petschek, H. E. (1966). Limit on stably trapped particle fluxes. *Journal of Geophysical Research*, *71*, 1–28.

Kivelson, M. G., & Southwood, D. J. (1996). Mirror instability II: The mechanism of nonlinear saturation. *Journal of Geophysical Research*, *101*, 17,365–17,372. https://doi.org/10.1029/96JA01407

Le Contel, O., Leroy, P., Roux, A., Coillot, C., Alison, D., Bouabdellah, A., … de la Porte, B. (2016). The search-coil magnetometer for MMS. *Space Science Reviews*, *199*, 257–282. https://doi.org/10.1007/s11214-014-0096-9

Leckband, J. A., Burgess, D., Pantellini, F. G. E., & Schwartz, S. J. (1995). Ion distributions associated with mirror waves in the Earth's magnetosheath. *Advances in Space Research*, *15*, 345–348. https://doi.org/10.1016/S0273-1177(99)80106-9

Lee, L. C., Wu, C. S., & Price, C. P. (1987). On the generation of magnetosheath lion roars. *Journal of Geophysical Research*, *92*(A3), 2343–2348. https://doi.org/10.1029/JA092iA03p02343

Lengyel-Frey, D., Farrell, W. M., Stone, R. G., Balogh, A., & Forsyth, R. (1994). An analysis of whistler waves at interplanetary shocks. *Journal of Geophysical Research*, *99*(A7), 13,325–13,334. https://doi.org/10.1029/94JA00781

Lindqvist, P.-A., Olsson, G., Torbert, R. B., King, B., Granoff, M., Rau, D., … Tucker, S. (2016). The spin-plane double probe electric field instrument for MMS. *Space Science Reviews*, *199*(1), 137–165. https://doi.org/10.1007/s11214-014-0116-9

Maksimovic, M., Harvey, C. C., Santolík, O., Lacombe, C., de Conchy, Y., Hubert, D., … Balogh, A. (2001). Polarisation and propagation of lion roars in the dusk side magnetosheath. *Annales Geophysicae*, *19*, 1429–1438. https://doi.org/10.5194/angeo-19-1429-2001

Masood, W., Schwartz, S. J., Maksimovic, M., & Fazakerley, A. N. (2006). Electron velocity distribution and lion roars in the magnetosheath. *Annales Geophysicae*, *24*, 1725–1735. https://doi.org/10.5194/angeo-24-1725-2006

Pollock, C., Moore, T., Jacques, A., Burch, J., Gliese, U., Saito, Y., … Zeuch, M. (2016). Fast plasma investigation for magnetospheric multiscale. *Space Science Reviews*, *199*, 1–76. https://doi.org/10.1007/s11214-016-0245-4

Rönnmark, K. (1982). *WHAMP: Waves in homogeneous, anisotropic, multicomponent plasmas, Kiruna Geophysical Institute, Report 179*. Kiruna, Sweden.

Russell, C. T., Anderson, B. J., Baumjohann, W., Bromund, K. R., Dearborn, D., Fischer, D., … Richter, I. (2016). The magnetospheric multiscale magnetometers. *Space Science Reviews*, *199*(1), 189–256. https://doi.org/10.1007/s11214-014-0057-3

Schwartz, S. J., Burgess, D., & Moses, J. J. (1996). Low-frequency waves in the Earth's magnetosheath: Present status. *Annales Geophysicae*, *14*, 1134–1150. https://doi.org/10.1007/s00585-996-1134-z

Sckopke, N., Paschmann, G., Bame, S. J., Gosling, J. T., & Russell, C. T. (1983). Evolution of ion distributions across the nearly perpendicular bow shock—Specularly and non-specularly reflected-gyrating ions. *Journal of Geophysical Research*, *88*, 6121–6136. https://doi.org/10.1029/JA088iA08p06121

Shevyrev, N. N., Zastenker, G. N., Eiges, P. E., & Richardson, J. D. (2006). Low frequency waves observed by Interball-1 in foreshock and magnetosheath. *Advances in Space Research*, *37*, 1516–1521. https://doi.org/10.1016/j.asr.2005.07.072

Smith, E. J., & Tsurutani, B. T. (1976). Magnetosheath lion roars. *Journal of Geophysical Research*, *81*, 2261–2266. https://doi.org/10.1029/JA081i013p02261

Smith, E. J., Holzer, R. E., & Russell, C. T. (1969). Magnetic emissions in the magnetosheath at frequencies near 100 Hz. *Journal of Geophysical Research*, *74*(11), 3027–3036. https://doi.org/10.1029/JA074i011p03027

Soucek, J., & Escoubet, C. P. (2011). Cluster observations of trapped ions interacting with magnetosheath mirror modes. *Annales Geophysicae*, *29*, 1049–1060. https://doi.org/10.5194/angeo-29-1049-2011

Southwood, D. J., & Kivelson, M. G. (1993). Mirror instability. I—Physical mechanism of linear instability. *Journal of Geophysical Research*, *98*, 9181–9187. https://doi.org/10.1029/92JA02837

Thorne, R. M., & Tsurutani, B. T. (1981). The generation mechanism for magnetosheath lion roars. *Nature*, *293*, 384–386. https://doi.org/10.1038/293384a0

Zhang, Y., Matsumoto, H., & Kojima, H. (1998). Lion roars in the magnetosheath: The geotail observations. *Journal of Geophysical Research*, *103*(A3), 4615–4626. https://doi.org/10.1029/97JA02519

Zimbardo, G., Greco, A., Sorriso-Valvo, L., Perri, S., Vörös, Z., Aburjania, G., … Alexandrova, O. (2010). Magnetic turbulence in the geospace environment. *Space Science Reviews*, *156*, 89–134. https://doi.org/10.1007/s11214-010-9692-5